Kinetic modeling of the direct synthesis of dimethyl ether over a CuO-ZnO-MnO/SAPO-18 catalyst and assessment of the CO_2 conversion

Ainara Ateka*, Javier Ereña, Javier Bilbao, Andrés T. Aguayo

Department of Chemical Engineering, University of the Basque Country UPV/EHU, P.O. Box 644, 48080 Bilbao, Spain

**Corresponding author*. Phone: +34 94 6015361; Fax: +34 94 6013500. E-mail address: ainara.ateka@ehu.eus (A. Ateka)

ABSTRACT

A kinetic model has been established for the direct synthesis of dimethyl ether (DME) from syngas and CO_2 feeds. The kinetic parameters have been determined fitting the experimental results obtained using a CuO-ZnO-MnO/SAPO-18 (CZMn/S) bifunctional catalyst in a fixed-bed isothermal reactor, under a wide range of operating conditions: 250-350 ºC; 10-40 bar; CO_2/CO molar ratio in the feed, between 0 and 1; H_2/CO_X molar ratio in the feed, 3/1 and 4/1; space time, from 1.25 $g_{cat}h(mol_C)^{-1}$, up to 20 $g_{cat}h(mol_C)^{-1}$; time on stream, up to 30 h. The model considers the kinetic equations of the individual reactions of methanol synthesis from CO and CO_2, the dehydration of methanol to DME, the water gas shift reaction (WGS) and the formation of paraffins, along with the deactivation kinetics. The attenuation of the reaction rates of methanol and paraffins synthesis has been considered by the competitive adsorption of CO_2 and H_2O in the metallic sites with respect to the adsorption of CO (more reactive than CO_2 in the synthesis of methanol). The deactivation by coke has been quantified by a kinetic equation dependent on the concentrations of methanol and DME, and the attenuation of the deactivation by the competitive adsorption of CO_2 and H_2O has also been

considered in this equation. The kinetic model allows predicting satisfactorily the evolution with time on stream of the concentration of the components in the reaction medium (methanol, DME, unreacted CO and CO_2, and paraffins formed as by-products). In addition, the model has been used to simulate the reactor, determining the effect of the reaction conditions on the conversion of CO_2. This conversion, in contrast to the yield of DME, increases with increasing CO_2 concentration in the reactor feed.

Keywords: DME synthesis, CO_2 conversion, syngas, kinetic model, catalyst deactivation

1. INTRODUCTION

Given the forecasts of growth of CO_2 emissions, up to a concentration of 570 ppm of CO_2 by the end of the 21st century, and in order to mitigate the devastating consequences of climate change, developed countries have adopted regulations to promote the efficient use of energy and the progressive replacement of fossil fuels by renewable sources (http://www.epa.gov/climatechange/ghgemissions/gases(co2.html), Climate change). In this scenario, the catalytic and electrocatalytic routes that use CO_2 as a raw material receive great attention, and especially the routes for fuel production, due to their potential capability for large-scale CO_2 valorization, through hydrogenation reactions (Fischer-Tropsch synthesis, synthesis of C_{2+} alcohols and of gasoline/isoparaffins among others) [1, 2]. Olah et al. [3] consider that the synthesis of dimethyl ether (DME) in a single stage co-feeding CO_2 together with syngas is an interesting alternative for replacing the industrial process for its production in two stages. These authors emphasize the environmental interest of this reaction when the syngas is produced from lignocellulosic biomass.

The main application of DME (CH_3-O-CH_3) nowadays is as domestic and automotive fuel, based on its properties (vapor pressure similar to that of liquefied petroleum gases, cetane number between 55-60) [4, 5] and the reduced emissions of NOx, SOx and particulate matter in its combustion [6, 7]. Based on a life cycle analysis (LCA), Lerner et al. [8] emphasize the interest of methanol and DME as clean transport fuels and determine that they can be economically competitive with oil derived fuels, due to the availability of natural gas. In addition, the economy of DME is also based on its future as intermediate raw material, progressively replacing petroleum derivatives and methanol for the production of olefins [9-13] or issoparaffin-rich gasoline [14] and as H_2 vector [15-20].

The synthesis of DME involves the following reactions:

Methanol synthesis: $CO + 2H_2 \leftrightarrow CH_3OH$ (1)

$CO_2 + 3H_2 \leftrightarrow CH_3OH + H_2O$ (2)

Methanol dehydration to DME: $2CH_3OH \leftrightarrow CH_3OCH_3 + H_2O$ (3)

Reverse water gas shift (rWGS): $CO_2 + H_2 \leftrightarrow CO + H_2O$ (4)

The secondary reaction of paraffins formation (mainly methane) also takes place:

$$nCO + (2n+1)H_2 \leftrightarrow C_nH_{2n+2} + nH_2O \quad (n=1\text{-}3) \qquad (5)$$

The interest of synthesizing DME from syngas (STD process), using bifunctional catalysts has grown in the last decade, due to several factors: i) the lower production cost of DME and methanol (byproduct) than the synthesis of methanol and the synthesis of DME in two stages [21]; ii) the possibility of producing syngas from different raw materials, such as coal, natural gas (from growing reserves), biomass and wastes from the consumer society (plastics, tires); iii) the promotion of the biomass gasification technology [22-24]. The most widely studied catalysts for the direct synthesis of DME use CuO-ZnO-Al_2O_3 (CZA) as metallic function [25], although Al_2O_3 has been completely or partially replaced by other metallic oxides, such as MnO or ZrO_2 [26], and ZnO (used to stabilize Cu) has been replaced by La_2O_3 [27] among others. For the acid function, catalysts of different porous structure are used (γ-Al_2O_3, silica-alumina, HZSM-5, NaHZSM-5, mordenite, HY, ferrierite, HMCM-22, SAPOs and ZrO_2). All those acid functions have in common a very low acid strength, a pursued characteristic in this process in order to avoid the formation of hydrocarbons [28]. Due to its relevance for the viability of the process, considerable attention has also been paid to the deactivation of the catalyst, whose main cause is considered to be the partial blockage of the metallic sites by coke [29], although coke formation is a consequence of

a synergy between the mechanisms in each function of the catalyst [30]. It has also been established that the increase in the H_2O content in the reaction medium attenuates coke deposition, due to the limitation of methoxy ions formation [31]. In addition, the catalyst is prone to irreversible deactivation, by Cu sintering above 300 °C [32].

Integrating methanol dehydration (Eq. 3) in the same reactor displaces the thermodynamic equilibrium of methanol synthesis (Eqs. 1 and 2), and allows to work at lower pressure, higher temperature and lower H_2/CO ratio in the feed than in the synthesis of methanol [33-35]. This latter advantage is important to valorize the syngas derived from biomass [3]. Besides, the lower thermodynamic limitation is favorable for the incorporation of CO_2 in the feed, increasing its conversion respect to that in the synthesis of methanol under the same conditions. However, the required conditions of pressure and temperature in the direct synthesis of DME are intermediate to the optimum conditions for the individual stages, and therefore, the direct synthesis requires catalysts and kinetic models suitable for these conditions. In addition, the incorporation of CO_2 in the feed has a remarkable influence on the composition of the reaction medium, as it leads to an increase in the content of H_2O in the reaction medium (by displacement of the WGS reaction, Eq. 4).

Among the initiatives on tailoring the catalysts used in the synthesis of DME to the conditions required when co-feeding CO_2 with syngas, the increase in the activity and stability of the CuO-ZnO sites of the CZA metallic function have been studied with different strategies. In this regard, the CO_2 hydrogenation rate has been improved substituting ZnO by Fe_2O_3 and using CeO_2 as promoter [36, 37]. The activity for the reverse WGS reaction (to potentiate the greater activity of CO than of CO_2) has been upgraded by substituting Al_2O_3 by MnO [38, 39], and ZrO_2 has been incorporated to increase the stability of the $Cu^{\delta+}$ sites [40-45]. The improvements in the acid function

have been addressed by reducing the hydrophilicity with respect to the conventionally used γ-Al_2O_3, which has been replaced by the HZSM-5 zeolite (modified for the passivation of its strong acid sites, responsible for the formation of hydrocarbons) [30, 46, 47], and silicoaluminophosphates (SAPO-18, SAPO-11) [26, 35, 48-51], among others (as WO_x/ZrO_2) [52].

In a previous work [26] the good performance of the CuO-ZnO-MnO (CZMn) metallic function and of the SAPO-18 (S) acid function in the valorization of CO_2 (co-fed together with syngas) has been verified, determining as optimal the mass ratio (metallic function)/(acid function) of 2/1 and emphasizing the lower cost of the CZMn/S catalyst and its regenerability [49]. In addition, relevant effects derived from the presence of CO_2 in the feed have been determined, which are essentially attributed to: i) the increase in the H_2O concentration, and ii) the relevance of the reverse WGS reaction (Eq. 4). Besides, it is important to point out that the adequate reaction conditions for the valorization of CO_2 correspond to those of lower production of DME, therefore, for the economic viability of the process a commitment between both objectives must be achieved [53]. The activity for the reverse WGS reaction (Eq. 4) is a key feature of the metallic function of the catalyst to achieve high CO_2 conversion values, since its conversion into CO is necessary (more active in the synthesis of methanol) to enhance DME yield [49, 54].

These features of the direct synthesis of DME must be taken into account in the design of suitable reactors. Among the reactors studied by means of simulation, multitubular fixed-bed reactors (used in the synthesis of methanol) [55] and fixed-bed reactors with hydrophilic membranes (to remove the formed H_2O and displace the limiting thermodynamic equilibrium of methanol synthesis and rWGS reactions) stand out [56, 57]. The design requires suitable kinetic models for CO_2 containing feeds and

reaction conditions. However, most studies regarding the kinetic modeling of the direct synthesis of DME [58, 59] have not been determined from experimental results of the direct synthesis of DME, but have been developed combining kinetic models previously established in the literature for the individual reactions of methanol synthesis [60, 61], methanol dehydration to DME [62, 63] and WGS reaction [64-74]. These kinetic models provide remarkable information on the mechanisms of the reactions considered and have allowed the design of industrial reactors for each of the mentioned reactions. Nevertheless, they are based on experimental results corresponding to the suitable conditions for each of these individual reactions, whereas the reaction conditions in the direct synthesis of DME and in particular when co-feeding CO_2 with syngas, are different. Thus, in the direct synthesis of DME, it is convenient to prepare the catalysts with an excess of acid function, in order to facilitate the progress of methanol dehydration, so that the overall reaction is conditioned by the progress of the methanol synthesis stage and by the WGS reaction. This characteristic of the catalyst prevents the advance of the overall reaction from being limited by the adsorption of H_2O on the acid function. It should also be noted that catalyst deactivation has not been considered in the kinetic modeling studies available in the literature.

In the present paper, a kinetic model has been established for the synthesis of DME over a CZMn/S catalyst (specifically suitable for the conversion of CO_2) [49] and this model has been used for the simulation of the reactor (isothermal fixed-bed), focusing on the valorization of the CO_2 co-fed together with syngas. This objective is complementary to the usual goal in the studies on the direct synthesis of DME, which are mainly addressed in the literature towards the maximization of the yield and selectivity of this product. Some fundamental aspects of the kinetic model (such as considering CO_2 co-feeding together with syngas, the effect of the high H_2O

concentration and the features of deactivation kinetics) have been established progressively in partial kinetic studies with different catalysts, of lower activity for the conversion of CO_2 and lower stability [34, 54, 75].

2. EXPERIMENTAL

2.1.Catalyst

The CuO-ZnO-MnO (CZMn) metallic function (for the synthesis of methanol) has been prepared by precipitation at pH= 7.0 and 70 ºC. The methodology is similar to that developed in previous works for the correct precipitation of the nitrates [76] starting from an aqueous solution of the corresponding nitrates (Cu, Zn, Mn) (1 M), with the desired 2:1:1.5 ratio of Cu:Zn:Mn and an aqueous solution of Na_2CO_3 (1 M). The following stages consist of aging the precipitate at 70 °C for 1 h, filtering and washing the precipitate to remove the remaining Na^+ ions, drying and calcination (300 °C, 10 h).

The SAPO-18 (S) acid function, has been prepared following the next steps: (i) precipitation of the precursor for the formation of the gel, by adding $Al(OH)_3 \bullet H_2O$ on an aqueous solution of H_3PO_4, and subsequently adding $C_8H_{19}N$ and SiO_2 to the mixture, under stirring for 1.5 h; (ii) crystallization of the mixture in a synthesis reactor (Highpreactor, Inycom) at 170 ° C and 200 bar for 6 days; and an additional day at room temperature for the aging of the suspension; (iii) filtering and washing of the suspension; (iv) drying and calcination at 550 °C for 5 h.

The CZMn/S bifunctional catalyst has been prepared by physical mixture of the metallic and acid functions. Bearing in mind that bifunctional catalysts for the STD process should be prepared in excess of acid function., a 2/1 mass ratio between the metallic and acid functions has been used [26]. The mixture has been finely powdered,

pelletized, crushed and sieved to select the desired particle size (125-500 μm). Prior to the reaction, the catalyst is subjected to a pre-treatment in situ in the reactor, consisting of a reduction in H_2 atmosphere, in two consecutive stages: 14 h at 200 ºC with a flow rate of 5 cm^3_{H2} min^{-1}, and 1.5 h at 300 ºC with a flow rate of 10 cm^3_{H2} min^{-1}. The H_2 is diluted in N_2, so that the total flow is 50 cm^3_{H2+N2} min^{-1}.

The Cu:Zn:Mn ratio of the metallic function (2: 0.75: 1.5) has been determined by X-ray fluorescence (Philips Minipal PW4025) and ICP-MS (Inductive Coupling Plasma-Mass Spectrometry). The most significant properties of the catalyst have been summarized in Table 1. The properties of the structure of micro and mesopores (BET surface area, micropore volume and pore volume) have been determined by N_2 adsorption-desorption (Micromeritics, ASAP 2010 system), and the metallic properties by selective chemisorption of N_2O (Autochem II 2920 coupled to a Pfeiffer-Vacuum OmniStar mass spectrometer). The acid properties (total acidity and average acid strength), combining thermogravimetry and calorimetry techniques to monitor the adsorption (at 150 ºC) -desorption of NH_3 (Setaram TG-DSC 111 with a Balzers Thermostar mass spectrometer on line), while the nature of the acid sites (Brönsted and Lewis) has been determined by FTIR spectrophotometry (Nicolet 6700, with a Specac catalytic chamber) in the 1400-1700 cm^{-1} region of pyridine adsorbed at 150 ºC. The structural and morphological properties have been determined by X-ray diffraction (Bruker D8 Advance), and by SEM and EDX (JEOL/JSM-7000f with a W filament and equipped with an Oxford Pentafet analyzer). The experimental techniques and the results of these analyzes have been described in detail in a previous work [26].

Table 1. Properties of the bifunctional CZMn/S catalyst.

Physical properties		
S_{BET} (m^2g^{-1})	V_m (cm^3g^{-1})	V_p (cm^3g^{-1})
213	0.060	0.278
Metallic properties		
S_{Cu} ($m^2g_{Cu}^{-1}$)	S_{Cu} ($m^2g_{Cat}^{-1}$)	Disp. (%)
112.0	22.0	17.3
Acid properties		
Acid strength (kJ/mol_{NH3})	Total acidity ($mmol_{NH3}/g$)	
99	0.12	

2.2. Reaction and analysis equipment and reaction conditions

The experiments have been carried out in an automated reaction equipment (PID Eng. & Tech. Microactivity Reference), described in detail in previous works [26, 50]. The equipment is provided with a fixed-bed reactor to operate at high pressure conditions and uses a specific software (Process@) to control the reaction conditions). The reactor is made of stainless steel 316, has an internal diameter of 9 mm and an effective length of 10 cm. It is located inside a ceramic chamber, heated by an electrical resistance and can operate up to 700 °C and 100 atm, with a limit catalyst mass around 5 g. The catalytic bed consists of a mixture of catalyst and an inert solid (SiC, carborundum of average particle size of 0.035 mm). The purpose of the dilution of the bed is: i) ensuring the isothermicity (avoiding hot spots), and; ii) reaching a suitable bed height to ensure an ideal flow in low space time conditions. The bed temperature is controlled by a TOHO TT-005 Series controller, and measured by two type K thermocouples, located in two longitudinal positions of the catalytic bed.

The on-line analysis of the samples has been conducted by diluting the product stream in a He (25 cm^3 min^{-1}) stream. The equipment used is a Varian-CP4900 micro-

chromatograph with three analytical modules, with the following columns: (i) Porapak Q (PPQ) (10 m), which separates CO_2, methane, ethane, propane, methanol, DME, water and butanes); (ii) molecular sieve (MS-5) (10 m) to separate H_2, CO, O_2 and N_2; and (iii) 5CB (CPSiL) (8 m), to identify the possible presence of C_5-C_{10} fraction. The identification and quantification of the compounds has been carried out based on calibration standards of known concentration.

In order to obtain experimental results for the kinetic modeling, the experiments have been carried out under the following reaction conditions: feed, H_2+CO+CO_2; 250-350 ºC; 10-40 bar; space time, 1.25-20 g_{cat} h mol_C^{-1}; time on stream, up to 30 h; CO_2/CO molar ratio, 0-1 (where 0 corresponds to the syngas feed); H_2/CO_x molar ratio, 3-4. It has been verified that under the experimental conditions used, the established theoretical criteria to avoid reactants and products (internal and external) diffusion restrictions in the catalyst particle is fulfilled [77]. Besides, these results have also been confirmed by means of experiments carried out with different particle sizes and feed flow rates, in which the results are reproduced.

3. RESULTS

The calculation stages of the kinetic model, in which the deactivation of the catalyst is considered, are described below. Subsequently, the model is used for the simulation of the reactor to determine the suitable conditions for the objectives of maximizing the yield of DME or the valorization of CO_2.

3.1. Methodology for data analysis

3.1.1. Kinetic parameters calculation

The methodology used for the analysis of the kinetic data is similar to that described in previous works regarding other catalytic processes with complex reaction schemes [78-80]. Toch et al. [81] have described the main stages for the kinetic modeling of those processes, without considering deactivation. Recently, Cordero-Lanzac et al. [82] have explained how to include the deactivation kinetics in the kinetic model. In the calculation, ideal flow, without radial gradients of concentration, and isothermal regime have been assumed, because the temperature differences between different radial and longitudinal positions are lower than 1 ºC. Consequently, the mass conservation equation of component *i*, at zero reaction time on stream (fresh catalyst) is:

$$r_{i,0} = \frac{dy_i}{d\left(W/F_0\right)} \quad (6)$$

where the concentration of each component *i*, y_i, is the molar fraction (in C units for the carbon containing compounds); W is the mass of catalyst; and F_0, the molar flow rate of C fed as CO and CO_2, in content C units.

The formation reaction rate of each component *i* at zero time on stream has been established considering the *n* reaction steps in which it is involved:

$$r_{i,0} = \sum^{n} (\upsilon_i)_j r_{j,0} \tag{7}$$

where $(\upsilon_i)_j$ is the stoichiometric coefficient of each *i* component in the *j* step of the kinetic scheme, and r_j is the rate of the *j* reaction step.

In first place, elementary reaction steps have been considered in Eq. 7. However, when the fitting resulted unsatisfactory, integer exponents have been tested for the concentration terms. In the reaction steps in which deactivation is considered, the reaction rate at time *t* has been defined as:

$$r_j = r_{j,0} \cdot a \tag{8}$$

The use of Eq. 8 requires a deactivation kinetic equation, which relates the activity with time, temperature and composition of the reaction medium. For this purpose, the following general expression has been defined:

$$-\frac{da}{dt} = \psi(T, p_i) a^d \tag{9}$$

where Ψ (T,p_i) is a function dependant on temperature and concentration of the components in the reaction medium precursors or inhibitors of coke.

The kinetic parameters of best fit for the model have been determined by multivariable non-linear regression, minimizing an error objective function defined as the weighted sum of residual squares between the experimental and calculated concentration values:

$$OF = \sum_{i=1}^{n_c} w_i \varphi_i = \sum_{i=1}^{n_c} w_i \sum_{k=1}^{n_e} (\bar{y}_{i,k}^{*} - y_{i,k})^2 \tag{10}$$

where, w_i is the weight factor for each component *i* of the kinetic scheme; φ_i is the total sum of squares for each component, including the repetitions in the same experimental condition; $\bar{y}^*_{i,k}$ is the average value of the composition of each component for the *k* experimental condition; $y_{i,k}$ is the corresponding value calculated by integrating the mass balance for component *i* in Eq. 6; n_c is the number of components in the kinetic scheme; and n_e is the total number of experimental conditions.

The parameters to be optimized are the kinetic constants of each *j* reaction, related to the temperature by the Arrhenius equation. To reduce the correlation existing between the preexponential factor and the activation energy, this equation has been reparameterized [83-86], expressing the kinetic constants as a function of its corresponding k_j^* at a reference temperature, T*:

$$k_j = k_j^* \exp\left[-\frac{E_j}{R}\left(\frac{1}{T}-\frac{1}{T^*}\right)\right] \tag{11}$$

When the kinetic equation includes parameters quantified in the equilibrium (thermodynamic equilibrium or adsorption of products and/or reactants), those are also reparameterized according to:

$$K_i = K_i^* \exp\left[\frac{\Delta H_i}{R}\left(\frac{1}{T}-\frac{1}{548}\right)\right] \tag{12}$$

Likewise, the constants of the deactivation equation have also been reparameterized. Therefore, according to this reparameterization, the kinetic parameters to be optimized are the kinetic constants and the equilibrium constants at reference temperature (275 ºC) and the corresponding activation energies, E_j, or reaction heats, ΔH_i. In addition, the

weight factor of each component has been calculated as the inverse of the average concentration in the studied condition range:

$$w_i = \frac{n_e}{\sum^{n_e} y_{i,k}} \tag{13}$$

where n_e is the number of experiments.

For determining the kinetic parameters of the model best fitting the experimental results, in Eq. 10, the expected values of the concentrations of each component, $y_{i,k}$, is calculated by integrating the mass balance for each *i* component in Eq. 6. For the integration of the kinetic equations and the multivariable non-linear regression a calculation program has been developed in MATLAB, where the main program gets the experimental data of the components in the kinetic scheme and assigns initial values to the parameters to be estimated and subsequently uses the multivariable non-linear regression routine. The usual procedure for determining the parameters of best fit consisted of a first approach to the optimum by means of the *genetic algorithm* subroutine [87]; followed by a second approach to the optimum with the subroutine *fminsearch* (provided by MATLAB); and finally using the *aju_mul* subroutine developed by the user (based on the Levenberg-Marquardt method) for calculating the confidence intervals of the parameters to be optimized. These subroutines, use the integration subroutine for the calculation of the compositions and activity (equal to one when calculating the parameters of the kinetic equations at zero time on stream) in the different experimental conditions and for each point of the mesh.

3.1.2. Significance and validity of the model

In order to verify the significance of the kinetic model, a variance analysis has been carried out, considering two properties of the overall sum of residual squares: the lack

of fit of the model and the dispersion of the experimental data. The ideal fit is reached when the lack of fit of the model is similar to the experimental error. Therefore, the relationship of the variances of the lack of fit, s_a^2, and of the experimental error, s_e^2, are compared. This relationship follows a Fisher distribution, with the corresponding ν_a and ν_e degrees of freedom.

$$F = \frac{s_a^2}{s_e^2} < F_{1-\alpha}(\nu_a,\nu_e) \tag{14}$$

Fulfilling Eq. 14 implies that the variance of the lack of fit is similar to the variance of the experimental error and therefore, the model represents satisfactorily the experimental data and does not require further improvement. The critical value of the Fisher function, $F_{1-\alpha}(\nu_a,\nu_e)$, has been determined for an established confidence percentage, 100 (1-α), for $\alpha = 0.05$, with the tables of Fishers distribution function, whereas the variances s_a^2 and s_e^2 are calculated from the values of the sum of squares of the errors and the degrees of freedom. s_e^2 has been calculated by fitting the results obtained in repeated runs for three components (DME, methanol and paraffins).

Following a similar variance analysis, the fitting improvement obtained with other models of different complexity (simpler models with less kinetic parameters, and more complex models, thus, involving more kinetic parameters) has been assessed in preliminary studies. This methodology, allows comparing different models by pairs, and determining whether the fitting improvement achieved with the most complex model over that obtained with the simplest model is significant. That is, for two models (a, b), with (ν_a,ν_b) degrees of freedom, respectively, being $s_a^2 > s_b^2$ with $SSE_a > SSE_b$ sum of square errors, the improvement obtained with model b (complex) over that obtained with model a (simple) is significant if Eq. 15 is fulfilled:

$$F_{a\text{-}b} = \frac{(SSE_a - SSE_b)/SSE_b}{(\nu_a - \nu_b)/\nu_b} > F_{1-\alpha}((\nu_a - \nu_b), \nu_b) \quad (15)$$

3.2. Kinetic model

3.2.1. Kinetic equations of the reaction steps

The following kinetic equations have been proposed for the individual reactions of the reaction scheme:

Methanol synthesis by CO and CO_2 hydrogenation (Eqs. 1 and 2, respectively):

$$r_{MeOH} = k_1 \left[p_{H_2}^2 p_{CO} - \frac{p_{CH_3OH}}{K_1} \right] \theta \quad (16)$$

$$r'_{MeOH} = k'_1 \left[p_{H_2}^3 p_{CO_2} - \frac{p_{CH_3OH} p_{H_2O}}{K'_1} \right] \theta \quad (17)$$

Methanol dehydration to DME (Eq. 3):

$$r_{DME} = k_2 \left[p_{CH_3OH}^2 - \frac{p_{CH_3OCH_3} p_{H_2O}}{K_2} \right] \quad (18)$$

WGS reaction (CO_2 formation) (Eq. 4):

$$r_{CO_2} = k_3 \left[p_{CO} p_{H_2O} - \frac{p_{CO_2} p_{H_2}}{K_3} \right] \quad (19)$$

Hydrocarbons formation (C_1-C_4 paraffins) (Eq. 5):

$$r_{HC} = k_4 \left[p_{H_2}^3 p_{CO} - \frac{p_{CH_4} p_{H_2O}}{K_4} \right] \theta \quad (20)$$

It should be noted that Eqs. 16 - 20 have been established by considering elementary reactions and the stoichiometry of hydrocarbon formation (Eq. 20) corresponds to the formation of CH_4 (main hydrocarbon). In addition, based on a preliminary study on the

relevance of the individual reactions, it has been found that the contribution of CO_2 to the synthesis of methanol (Eq. 17) is below 1 % of the contribution of CO, under the most favorable conditions. Consequently, in order to simplify the kinetic model, the direct synthesis of methanol from CO_2 has not been taken into account. This result is relevant, because it indicates that the conversion of CO_2 into methanol under the conditions of direct synthesis of DME, takes place by its transformation into CO, through the reverse WGS reaction (Eq. 4). Ateka et al. [88] have emphasized the relevance of the activity of the metallic function of the catalyst for the reverse WGS reaction on the valorization of CO_2. On the other hand, a factor (θ) has been included in the methanol and hydrocarbons formation kinetic equations (Eqs. 16, 17 and 20). This term, Eq. 21, quantifies the attenuation of the reaction rates of the steps activated by the metallic function, as a consequence of the competition for the adsorption of H_2O and CO_2 with CO in the metallic sites. In this regard, it has been determined in a preliminary study for model discrimination, that considering this term in the WGS reaction does not lead to any significant improvement in the fitting. Predictably, the reaction rate of methanol dehydration could also be attenuated by the adsorption of H_2O in the acid sites of SAPO-18, but this will have no effect on the results, because the catalyst has been prepared with excess of acid function, so that the limiting step in the synthesis of DME is the synthesis of methanol. Ereña et al. [54] considered the adsorption of H_2O in the kinetics of methanol synthesis and in this work, in which CO_2 is co-fed with syngas, it has been demonstrated that the fitting of the results to the kinetic model also requires the consideration of the adsorption of CO_2 in the metallic sites.

$$\theta = \frac{1}{1 + K_{H_2O} p_{H_2O} + K_{CO_2} p_{CO_2}} \tag{21}$$

Using the methodology described in Section 3.1.2., it has been verified that fitting the experimental results requires considering both terms of H_2O and CO_2 concentration in the denominator of Eq. 21.

3.2.2. Deactivation kinetic equation

The deactivation of the catalyst affects the synthesis of methanol (since the acid function is in excess) and is mainly due to the deposition of coke on the metallic sites [88]. In a previous study conducted using a CuO-ZnO-Al_2O_3/γ-Al_2O_3 catalyst [29] this coke deposition has been related to the condensation to polyaromatics of the hydrocarbons formed from methoxy ions, which are intermediates in the dehydration of methanol, but also in the secondary reactions of hydrocarbon formation. Thus, upon increasing the CO_2 content in the reaction medium H_2O concentration increases (the reverse WGS is favored, Eq. 4), which attenuates the rate of methoxy ion formation and justifies the decrease in the formation of coke [31]. Besides, a synergistic effect of the metallic and acid sites of the catalyst to favor the mechanisms of coke formation has been established [30]. Considering deactivation, and bearing in mind that the contribution of CO_2 hydrogenation to methanol has been determined to be negligible over that of CO, the rate of methanol synthesis is quantified as:

$$r_{MeOH} = k_1\left[p_{H_2}^2 p_{CO} - \frac{p_{CH_3OH}}{K_1}\right]\theta\, a \tag{22}$$

The deactivation kinetic equation (Eq. 23) has been established considering both the aforementioned role of the concentration of oxygenates (methanol and DME) in the formation of methoxy ions (precursors of coke) and the attenuating role of H_2O and CO_2 in the formation mechanisms of these ions.

$$-\frac{da}{dt} = \frac{k_d(p_{MeOH} + p_{DME})}{1 + (K_{H_2O})_d\, p_{H_2O} + (K_{CO_2})_d\, p_{CO_2}} a^d \tag{23}$$

Again, using the methodology explained in Section 3.1.2, it has been verified that the fitting to the experimental results, considering catalyst deactivation, is not significantly improved considering the effect of H_2O and CO_2 concentrations with more complex expressions.

3.2.3. Kinetic parameters

Table 2 gathers the values of the calculated kinetic parameters of best fit and the statistical parameters (objective function, Eq. 10 and residual variance). Table 3 summarizes the parameters for the significance test of the model (sum of squares of the errors, number of degrees of freedom, variance of the experimental error and the variance of the lack of fit of the kinetic model, along with the ratio of variances and the critical value of Fisher's function). The results show that the model satisfies the required significance test, since the error related to the lack of fit is comparable to the experimental error.

The values of the kinetic parameters listed in Table 2 reveal that the kinetic constant of methanol dehydration (at reference temperature), k_2^*, is remarkably higher than that of methanol synthesis, k_1^* (7.38 mol $g_{cat}^{-1}h^{-1}bar^{-2}$ over $1.40 \cdot 10^{-5}$ mol $g_{cat}^{-1}h^{-1}bar^{-3}$), which is the slowest step. Moreover, the high value of the kinetic constant k_3* evidences the relevance of the WGS reaction in this process, while the kinetic constant of paraffin formation, k_4^*, is even lower than k_1* for methanol synthesis from CO, but its value is important due to its presumable relationship with the formation of coke. In addition, the activation energy of methanol synthesis from CO, E_1, is four times higher than that of methanol dehydration to DME (E_2), which is in accordance with the relevant effect of the temperature in the results of CO conversion and consequently of CO_2 conversion. Moreover, the activation energy, E_4, of the hydrocarbon formation reaction is remarkably higher than that of methanol synthesis. On the other hand, at low

temperature, the role of the competitive adsorption of CO_2 on the attenuation of the methanol synthesis and WGS reactions is more important than that of H_2O adsorption (higher equilibrium constant at reference temperature), but this relative importance reverses when increasing temperature. It is also noteworthy, the low value of the activation energy of the deactivation, E_d; and the greater attenuation of the deactivation by the H_2O in the reaction medium than by the CO_2 ($(K_{H2O})_d^* > (K_{CO2})_d^*$). It should be noted that even if the value of the activation energy of the WGS reaction is within the values reported in the literature [64-74], the activation energies of the different reaction stages are lower than those obtained in the literature for the individual reactions of methanol synthesis [60, 61] and methanol dehydration to DME [62, 63, 89, 90]. This difference relies on the degree of empiricism of the kinetic expressions established (Eqs. 16-23), in order to consider the different reactions involved, deactivation and the complex role of H_2O in the reaction medium, which gives way to apparent values of the activation energies. However, those values are within the ranges reported in the literature for kinetic models established for the direct DME synthesis process, over different catalysts; as Moradi et al. establishing 115 and 81 kJ mol^{-1} for methanol synthesis and dehydration, respectively, over CZA/HZSM-5 bifunctional catalysts [59], or 66 and 69 kJ mol^{-1} reported by Hadipour and Sohrabi [91] for CZA/γ-Al_2O_3 catalyst from syngas feeds, or 90 and 231 kJ mol^{-1} by Ereña et al. [54] over similar catalysts using H_2+CO_2 feeds.

Table 2. Kinetic parameters and statistical parameters of the experimental results.

Kinetic parameter		
k_1^*	$mol_{MeOH}\ g_{cat}^{-1}\ h^{-1}\ bar^{-3}$	$1.40\ (\pm 0.21)10^{-5}$
k_2^*	$mol_{DME}\ g_{cat}^{-1}\ h^{-1}\ bar^{-2}$	$7.38\ (\pm 0.65)$
k_3^*	$mol\ g_{cat}^{-1}\ h^{-1}$	$46.5\ (\pm 0.22)$
k_4^*	$mol_{HC}\ g_{cat}^{-1}\ h^{-1}\ bar^{-4}$	$1.90\ (\pm 0.30)10^{-9}$
E_1	$kJ\ mol^{-1}$	$72.3\ (\pm 2.35)$
E_2	$kJ\ mol^{-1}$	$17.2\ (\pm 0.35)$
E_3	$kJ\ mol^{-1}$	$91.0\ (\pm 0.35)$
E_4	$kJ\ mol^{-1}$	$219.4\ (\pm 5.0)$
K_{H2O}^*	bar^{-1}	$2.08\ (\pm 0.27)10^{-3}$
K_{CO2}^*	bar^{-1}	$6.01\ (\pm 0.56)10^{-2}$
ΔH_{H2O}	$kJ\ mol^{-1}$	$231.9\ (\pm 4.4)$
ΔH_{CO2}	$kJ\ mol^{-1}$	$71.9\ (\pm 2.3)$
k_d^*	$h^{-1}\ bar^{-1}$	$1.43\ (\pm 0.22)\ 10^{-3}$
E_d	$kJ\ mol^{-1}$	$20.6\ (\pm 0.90)$
$(K_{H2O})_d^*$	bar^{-1}	$2.62\ (\pm 0.25)10^{-3}$
$(K_{CO2})_d^*$	bar^{-1}	$3.20\ (\pm 0.30)10^{-4}$
$(\Delta H_{H2O})_d$	$kJ\ mol^{-1}$	$50.6\ (\pm 1.5)$
$(\Delta H_{CO2})_d$	$kJ\ mol^{-1}$	$62.7\ (\pm 1.3)$
d		$0.31\ (\pm 0.05)$
OF		$7.46\ 10^{-1}$
Residual variance		4.58

Table 3. Parameters for the variance analysis of the kinetic model.

	Experimental. (e)	Model (a)
ν	18	18
s^2	$1.63 \cdot 10^{-3}$	$3.11 \cdot 10^{-3}$
s_a^2/s_e^2	1.85	
$F_{1-\alpha}(\nu_a,\nu_e)$	1.95	
Significance test	Valid	

3.4. Fitting of the kinetic model to the experimental results

3.4.1. *Product concentration at zero time on stream*

The quality of the kinetic model to determine the effect of the reaction conditions on products distribution at zero time on stream is ascertained in Figs. 1-3, in which the experimental results (points) of the evolution of the concentration (mole fraction) of each component of the reaction medium with space time and the values calculated with the model (lines) are compared. The results (taken as an example) correspond to different CO_2/CO molar ratios in the feed (0, 1/3 and 2/3), and to different particular conditions.

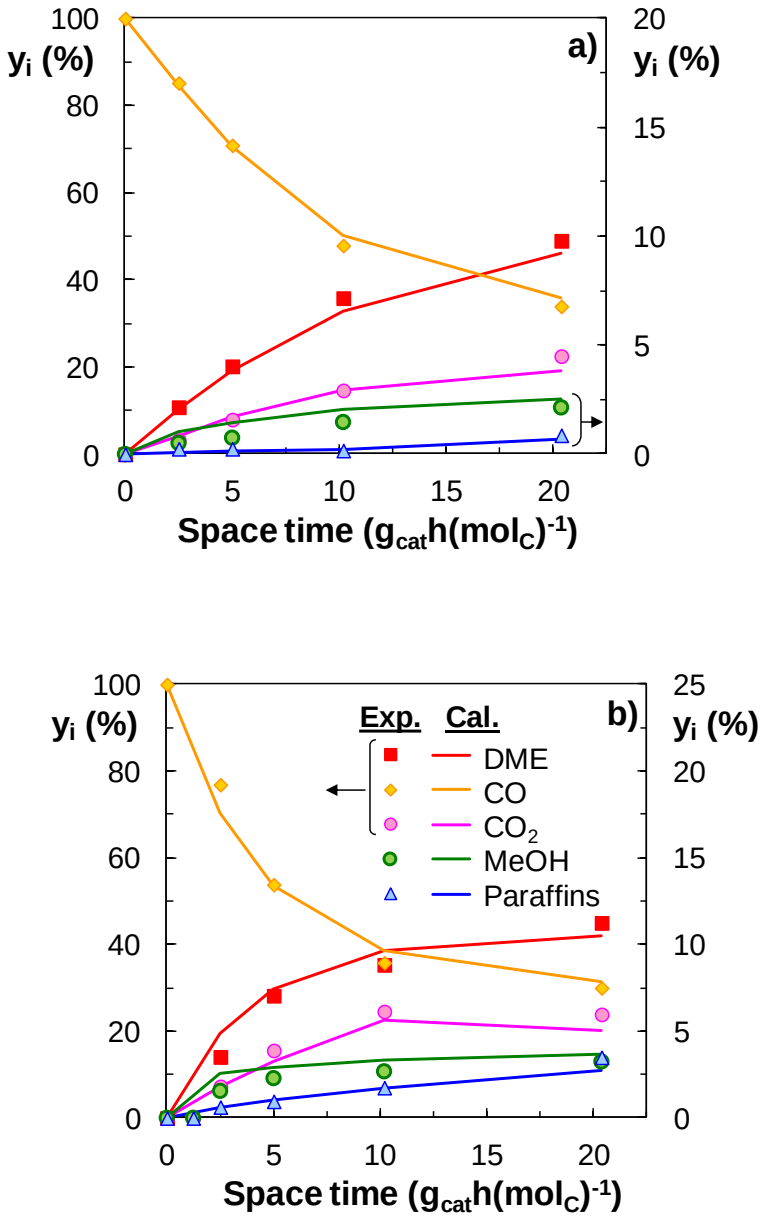

Fig. 1. Comparison of the evolution with space time of the experimental values of product concentration at zero time on stream (points) and those calculated using the kinetic model (lines), at 275 ºC (a) and 300 ºC (b). Reaction conditions: 30 bar; feed, $CO+H_2$; H_2/CO_x, 3.

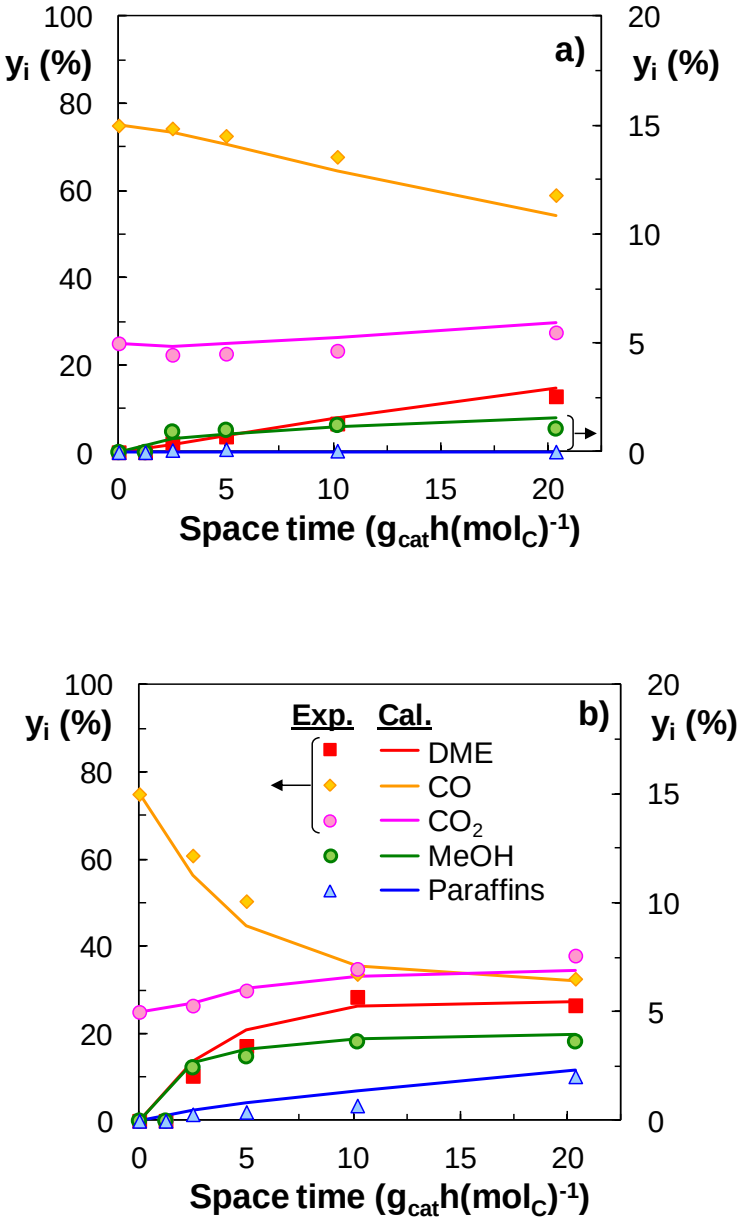

Fig. 2. Comparison of the evolution with space time of the experimental values of product concentration at zero time on stream (points) and those calculated using the kinetic model (lines), at 250 ºC (a) and 300 ºC (b). Reaction conditions: 30 bar; feed, $CO+H_2+CO_2$; $CO_2/CO=1/3$; H_2/CO_x, 3.

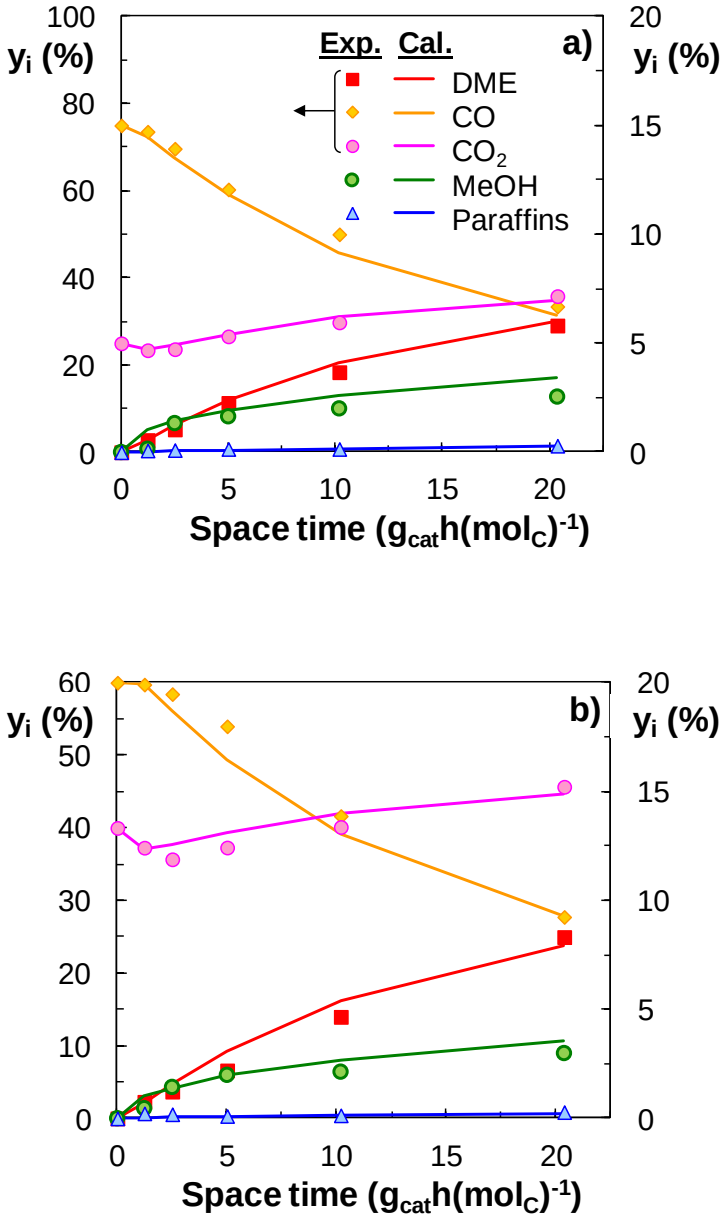

Fig. 3. Comparison of the evolution with space time of the experimental values of product concentration at zero time on stream (points) and those calculated using the kinetic model (lines), for CO_2/CO= 1/3 (a) and CO_2/CO= 2/3 (b). Reaction conditions: 275 ºC; 30 bar; feed, $CO+H_2+CO_2$; H_2/CO_x, 3.

3.4.2. Evolution of product concentration and yield with time on stream

As depicted in Fig. 4 as an example, where the values of products concentrations obtained with the kinetic model (lines) taking into account the deactivation kinetics are compared with the experimental values (points), it has been proven that the model fits satisfactorily its evolution with time on stream. The study has been extended and Figs. S1-S4 in the *Supplementary Information* show more comparisons between the calculated and experimental values, at 5 h time on stream.

Product yield has been determined as:

$$Y_i = \frac{n_i \cdot F_i}{F^0_{CO_x}} 100 \qquad (23)$$

where n_i is the number of C atoms in a molecule of component *i*; F_i the molar flowrate of component *i* at the reactor outlet stream; and F^0_{COx} is the molar flowrate of CO_x ($CO+CO_2$) in the feed.

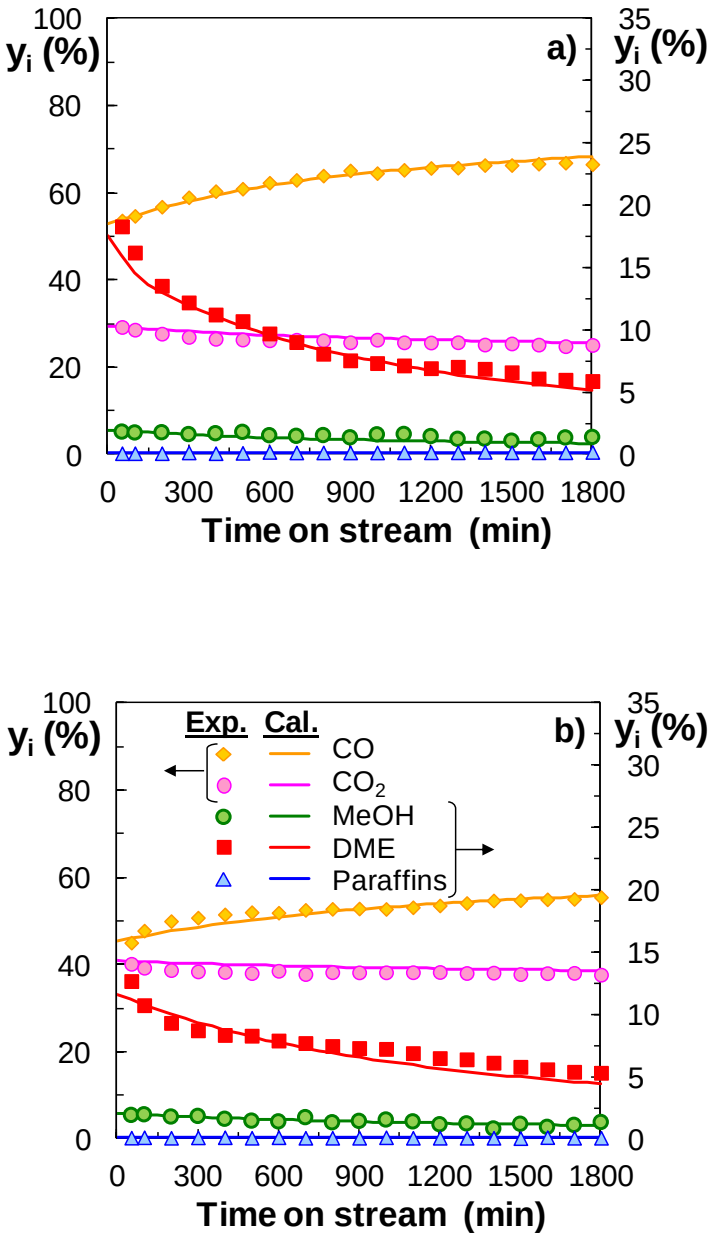

Fig. 4. Comparison of the evolution with time on stream of the experimental values of product concentration (points) and those calculated using the kinetic model (lines), for CO_2/CO = 1/3 (a) and CO_2/CO = 2/3 (b). Reaction conditions: 275 ºC, 30 bar; 10.18 $g_{cat}h(mol_C)^{-1}$; H_2/CO_x, 3.

3.5. Simulation of the reactor and CO_2 valorization

The results of the previous section have shown that the kinetic model is suitable for determining products distribution and their evolution with time on stream in a wide range of operating conditions. Consequently, the kinetic model has been used to simulate the isothermal fixed-bed reactor, with the aim of exploring the capability of the direct DME synthesis process to valorize CO_2. This objective differs from the usual one in the literature, as most of the studies are focused on maximizing the yield of DME. However, the perspective of valorizing CO_2 requires analyzing the capacity of the reaction for this purpose. In addition, it must be taken into account that CO_2 is a by-product of the WGS reaction (Eq. 4) in the synthesis of DME, so that minimizing its emission also has a high environmental interest. On the other hand, it must be taken into account that the economic viability of the process requires operating under conditions in which a compromise is reached between the yield of DME and the net conversion of CO_2. Therefore, to deepen in the knowledge of the capability of the direct synthesis of DME for these two targets, operating maps (with temperature and space time as coordinates) that allow identifying the most suitable operating conditions have been determined. The simulation of the isothermal fixed-bed reactor has been carried out using a calculation program written in MATLAB, which has been explained schematically in the *Supplementary Information* (Figs. S5 and S6). The main program gets the starting data; i) temperature, pressure, CO_2/CO and H_2/CO_x ratios; ii) the values of the kinetic parameters (Table 2), and; iii) the time on stream and space time vectors in the interval to be studied. Next, a subroutine integrates the differential equations system defined in secondary subroutines, to calculate the composition of the reactor outlet stream and the activity of the catalyst under the different conditions. As a result,

the program allows determining the evolution of products yield and CO_2 conversion with space time and with time on stream. CO_2 conversion has been defined as:

$$X_{CO_2} = \frac{F^0_{CO_2} - F_{CO_2}}{F^0_{CO_2}} 100 \quad (24)$$

where F^0_{CO2} and F_{CO2} are the molar flow rates of CO_2 in the feed and in the product stream.

Figs. 5-7 show the simulation results. Each figure corresponds to a CO_2/CO ratio (1/3, 1 and 5, respectively). Graphs a) show the evolution of CO_2 conversion with space time and time on stream, for fixed values of the other reaction conditions (275 ºC, 30 bar, H_2/CO_x= 3). In graphs b) operation maps are shown, where the values of space time and time on stream are related to reach a certain value of CO_2 conversion. In Fig. 5b, corresponding to a CO_2/CO ratio of 1/3, the CO_2 conversion is negative for space time values above 2 $g_{cat}h\ (mol_C)^{-1}$, which indicates that under these conditions CO_2 is formed in the reaction (resulting from the WGS reaction, Eq. 4). Below this value of space time CO_2 conversion is positive, as in all the conditions of Figs. 6b and 7b. Thus, the results highlight that the CO_2/CO ratio in the feed conditions the required reaction conditions to enhance CO_2 conversion. Indeed, it is observed that by increasing the CO_2/CO ratio in the feed, the space time interval in which the CO_2 conversion is maximum is wider. For low CO_2/CO ratio in the feed (for the lowest value in the range studied, CO_2/CO = 1/3) (Fig. 5), the maximum CO_2 conversion (around 3 %) is obtained with small time space value, around 1 $g_{cat}h\ (mol_C)^{-1}$. Increasing the space time above this value hinders the conversion of CO_2, since its formation increases with increasing space time.

For the ratio CO_2/CO = 1 (Fig. 6), the maximum CO_2 conversion is of 7 % and is obtained in a space time interval within 1 and 2 $g_{cat}h\ (mol_C)^{-1}$. By increasing the

CO_2/CO ratio to 5 (Fig. 7), a greater CO_2 conversion is obtained (reaching a 15 % at these conditions) in the 4 - 10 $g_{cat}h\ (mol_C)^{-1}$ range.

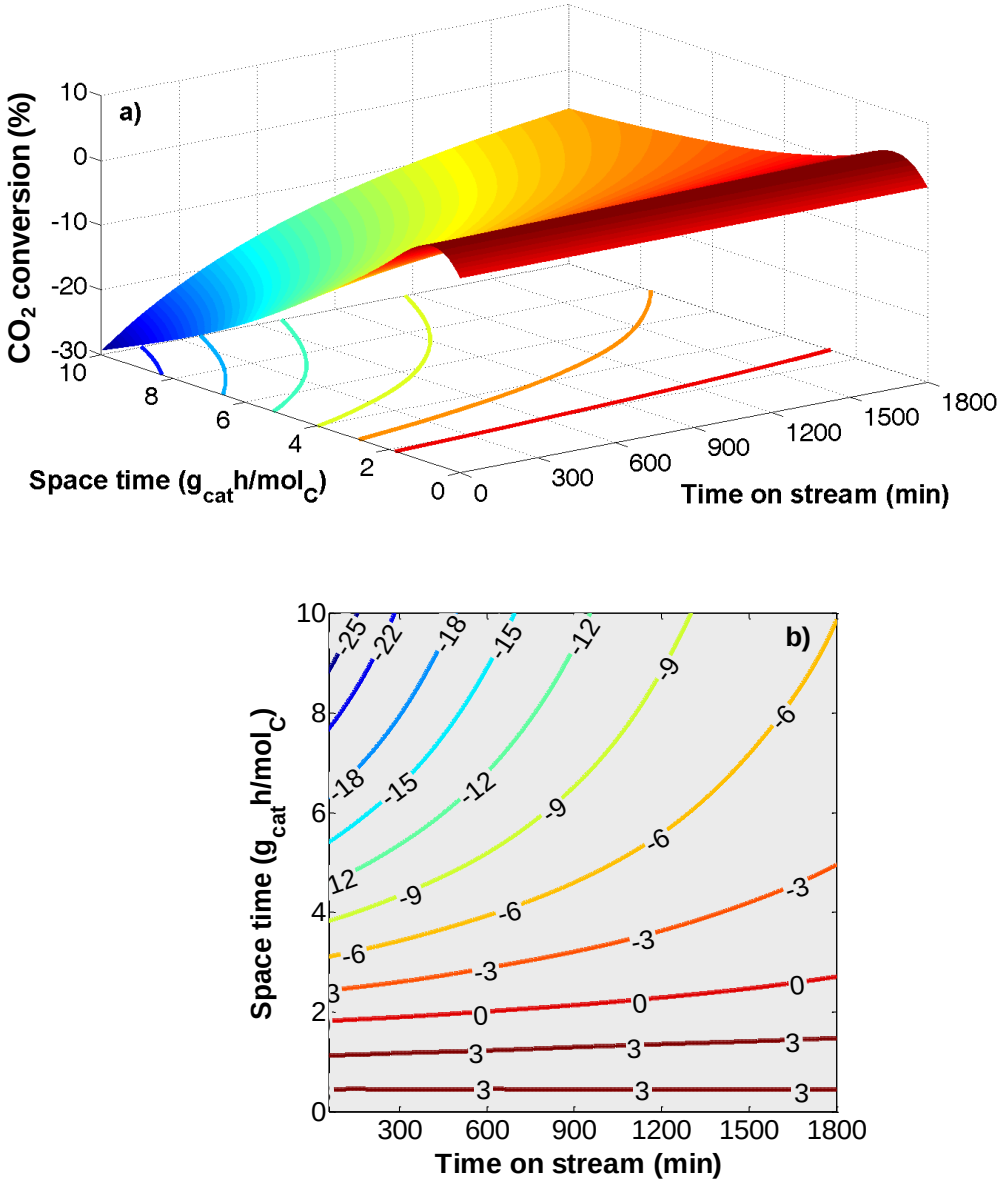

Fig. 5. Evolution of CO_2 conversion with space time and time on stream (a) and curves of equal conversion conditions (b), for CO_2/CO = 1/3. Reaction conditions: 275 ºC, 30 bar; 10.18 $g_{cat}h(mol_C)^{-1}$; H_2/CO_x, 3.

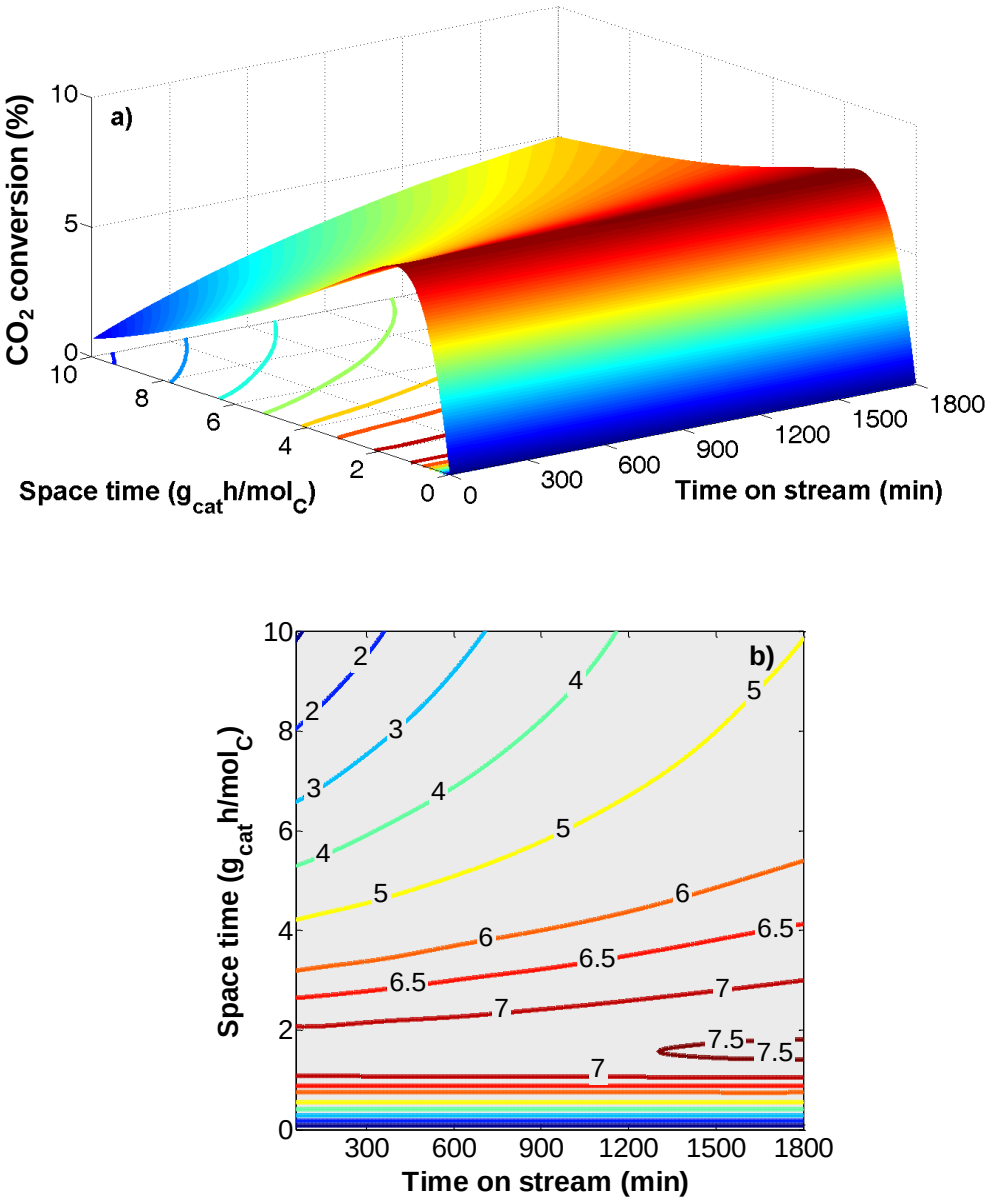

Fig. 6. Evolution of CO_2 conversion with space time and time on stream (a) and curves of equal conversion conditions (b), for CO_2/CO = 1. Reaction conditions: 275 ºC, 30 bar; 10.18 $g_{cat}h(mol_C)^{-1}$; H_2/CO_x, 3.

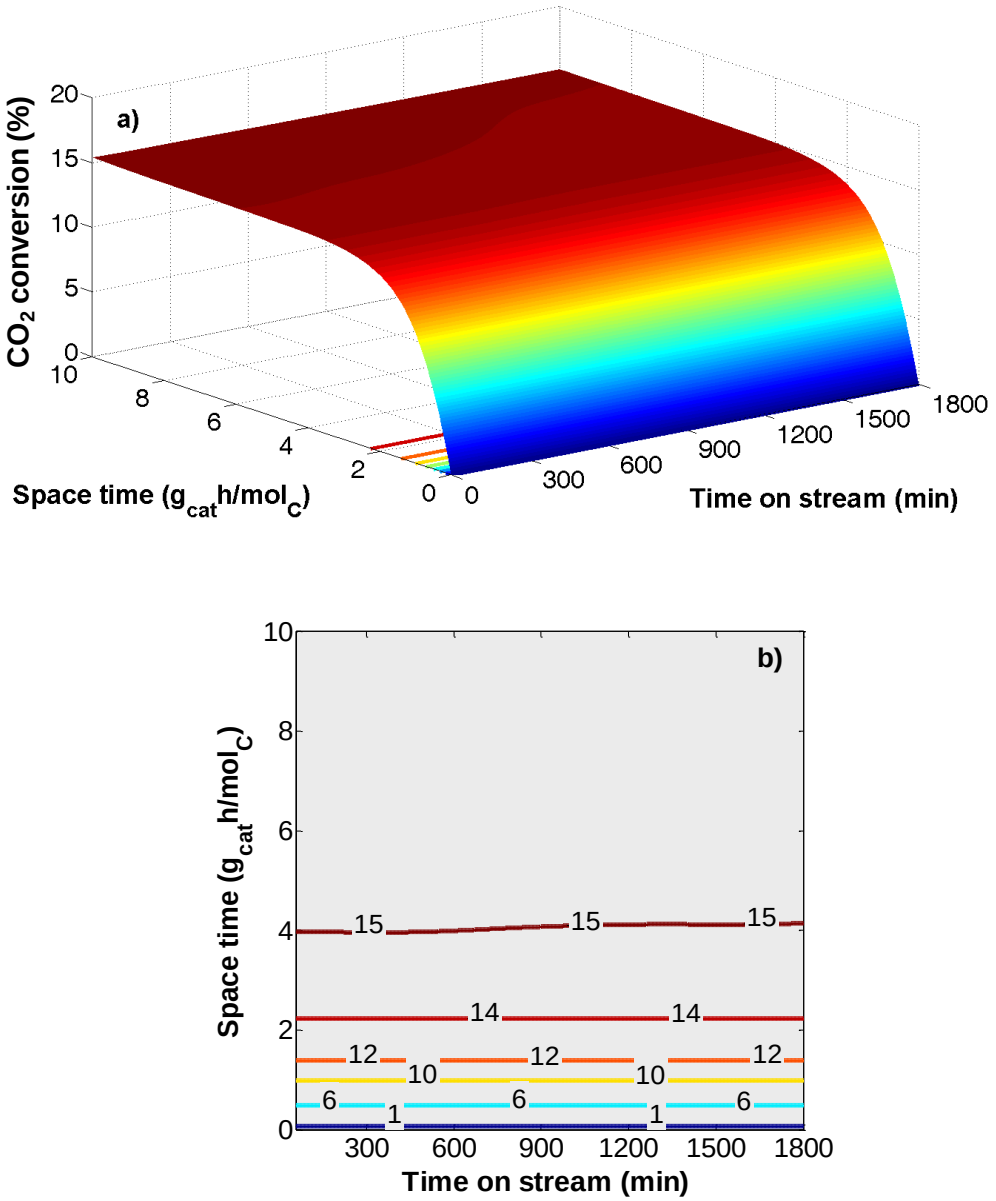

Fig. 7. Evolution of CO_2 conversion with space time and time on stream (a) and curves of equal conversion conditions (b), for CO_2/CO = 5. Reaction conditions: 275 ºC, 30 bar; 10.18 $g_{cat}h(mol_C)^{-1}$; H_2/CO_x, 3.

On the other hand, it is observed in Fig. 7b (for $CO_2/CO = 5$) that for a high CO_2/CO ratio, deactivation is attenuated and CO_2 conversion is almost constant with time on stream. Nevertheless, for $CO_2/CO = 1/3$ (Fig. 5b) and 1 (Fig. 6b) and for high values of space time, the conversion of CO_2 increases with time on stream, as a consequence of the deactivation of the catalyst under these conditions.

However, as mentioned previously, the co-feeding of CO_2 together with syngas has an unfavorable effect of decreasing the yield of DME, which must be taken into account. The aforementioned results have highlighted these opposite trends of CO_2 conversion and DME yield, to the point that the deactivation of the catalyst for DME synthesis favors the conversion of CO_2. Hence, for further studying these trends, the results of CO_2 conversion obtained for different values of the CO_2/CO ratio and space time have been plotted together with the yield of DME (Fig. 8). It is observed that the increase of the CO_2/CO ratio in the feed favors the conversion of CO_2 for a certain value of space time, but decreases the production of DME. On the other hand, for a given CO_2/CO ratio (lower than $CO_2/CO = 5$), increasing the conversion of CO_2 requires working at low space time values, resulting in a decrease in the yield of DME. For CO_2/CO values above 5, this trend is reversed and the increase in space time not only enhances CO_2 conversion but also slightly favors the yield of DME, which is interesting for the viability of the process focusing on the objective of maximizing CO_2 conversion as a priority. It should be noted that these simulation results, using the kinetic model, are consistent with the trends established by the thermodynamic analysis of the CO_2 hydrogenation to methanol and DME, which predict that the direct DME synthesis has lower thermodynamic limitations than methanol synthesis, and that higher CO_2 conversion is obtained upon increasing the content of CO_2 in the feed, at suitable operating conditions (below 300 ºC) [35,92]. Besides, the results also evidence the

relevance of having an accurate kinetic model to establish the suitable conditions for a good compromise between CO_2 conversion and DME yield.

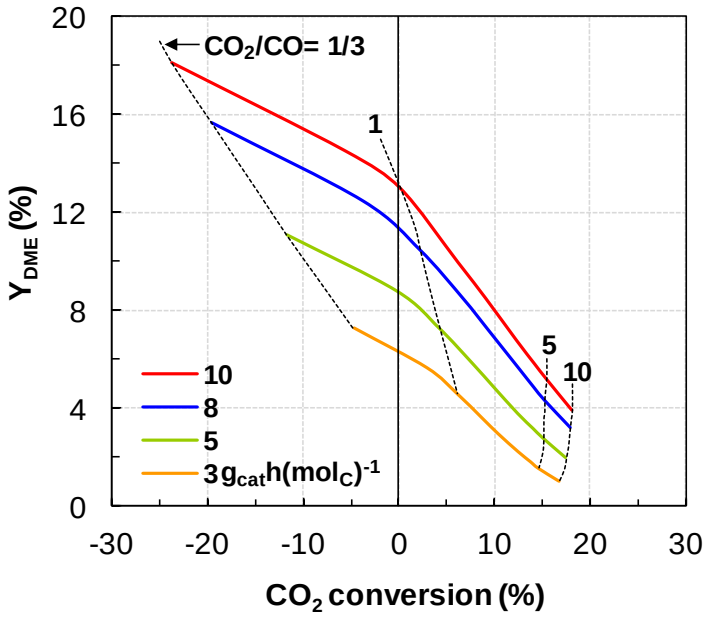

Fig. 8. Relationship between CO_2 conversion and DME yield at zero time on stream, for different values of the CO_2/CO ratio in the feed and space time. Reaction conditions: 275 ºC, 30 bar; 5 h time on stream; H_2/CO_x, 3.

CONCLUSIONS

It has been proven that the proposed kinetic model is useful to quantify products distribution (methanol, DME, CO, CO_2, and hydrocarbons) and its evolution with time on stream in the direct synthesis of DME from mixtures of CO_2 and syngas. The model predicts the results for a wide range of conditions (250-350 ºC; 10-40 bar; space time, up to 20 $g_{cat}h$ $(mol_C)^{-1}$; CO_2/CO molar ratio, up to 1; and, H_2/CO_x molar ratio up to 4). Furthermore, under these conditions the catalyst has high activity, selectivity to DME and stability.

The values of the kinetic parameters of the model show that the synthesis of methanol is the controlling step, and that the dehydration of methanol is remarkably faster (being k_2* five orders of magnitude higher than k_1*). On the other hand, the activation energies of methanol synthesis and hydrocarbons formation are way larger than that of methanol dehydration reaction. Among the characteristics of the model, the need to consider the competitive adsorption of CO_2 and H_2O in the metallic sites, attenuating the rate of methanol synthesis and that of hydrocarbons formation must be underlined. The relative importance of the adsorption of the two components depends on the temperature, being greater that of CO_2 at low temperature, but making remarkable the relevance of the adsorption of H_2O upon increasing reaction temperature.

The deactivation kinetic model is in agreement with the hypothesis that the formation of coke on the metallic sites takes place with oxygenates (methanol and DME) as precursors of coke, with methoxy species (given their reactivity to form hydrocarbons) as active intermediates. Likewise, the model considers an attenuating effect of the deactivation by the H_2O and CO_2 in the reaction medium, the former being more important due to the control of the concentration of methoxy species.

The results give value to the thermodynamic forecasts of the capability of the direct synthesis of DME for the valorization of CO_2, whose conversion is strongly dependent on the CO_2/CO ratio, increasing as this ratio increases. Thus, for a CO_2/CO ratio of 1, the maximum conversion of CO_2 is 3 %, and 15 % for a CO_2/CO = 5. Under these conditions of high CO_2 content in the feed, it is noteworthy that increasing space time enhances both the CO_2 conversion and DME yield. However, for maximum CO_2 conversion conditions DME yield is low, which will require settling a balance between both objectives for the viability of the process.

ACKNOWLEDGMENTS

This work has been carried out with the financial support of the Ministry of Economy and Competitiveness of the Spanish Government and ERDF funds (CTQ2013-46173-R and CTQ2016-77812-R), the Basque Government (Project IT748-13). Ainara Ateka is grateful for the Ph.D. grant from the Department of Education, University and Research of the Basque Government (BFI09.69).

NOMENCLATURE

a activity.

CO_x $CO+CO_2$.

DME, MeOH dimethyl ether and methanol, respectively.

d deactivation order.

E_j activation energy of reaction *j* in the reaction scheme, kJ mol^{-1}.

F_i^0, F_i molar flow rate of compound i in the reactor inlet and outlet streams, respectively, in content C units.

ΔH_i, $(\Delta H_i)_d$ term related to the adsorption heat of component *i* in the kinetics at zero time on stream and in the deactivation kinetics, respectively, kJ mol^{-1}.

K_i, K_i^* term related to the adsorption equilibrium constant of component i (H_2O or CO_2) and its value at reference temperature, bar^{-1}.

$(K_i)_d$, $(K_i)_d^*$ term related to the adsorption equilibrium constant of component i (H_2O or CO_2) in the deactivation kinetics and its value at reference temperature, bar^{-1}.

K_1, K_1', K_2, K_3, K_4 equilibrium constants of the reactions of methanol synthesis from CO, from CO_2, methanol dehydration, WGS reaction and hydrocarbons synthesis, respectively.

K_j equilibrium constant for step *j* of the reaction scheme.

k_j, k_j^* kinetic constant for j reaction step and its value at reference temperature, respectively.

k_d, k_d^* deactivation kinetic constant and its value at reference temperature, bar^{-1} min^{-1}.

n, n_c, n_e number of reactions in the reaction scheme, of components and of experimental runs in the kinetic study, respectively.

n_i number of carbon atoms in each *i* component.

OF objective function.

P pressure, bar.

p_i partial pressure of component *i*, bar.

r_i, $r_{i,0}$ formation rate of component *i* at t and zero time on stream, respectively.

r_j, $r_{j,0}$ rate of reaction *j* in the reaction scheme at t and zero time on stream, respectively.

s_a^2, s_e^2 variance of the lack of fit and experimental error, respectively.

SSE sum of square errors of each model.

T, T* temperature and reference temperature, respectively, K.

W catalyst mass, g.

w_i weight factor for each *i* component inthe reaction scheme.

X_{CO2} CO_2 conversion, %.

Y_i yield of component *i*, %.

y_i molar fraction of component *i*.

$\bar{y}_{i,k}^*$, $y_{i,k}$ average value of the molar fraction of each *i* component in the k experimental condition, and the value calculated by integraton the mass balance, respectivamente.

Greek symbols

φ_i	sum of square residuals for each *i* component.
θ	term that quantifies the attenuation of the reaction rate by H_2O and CO_2 adsorption.
ν_a, ν_e	degrees of freedom.
$\nu_{i,j}$	stoichiometric coefficient of component *i* in reaction *j*.

REFERENCES

[1] E. Catizzone, G. Bonura, M. Migliori, F. Frusteri, G. Giordano, CO_2 recycling to dimethyl ether: State-of-the-art and perspectives. Molecules 23, (2018) 31.

[2] S. Roy, A. Cherevotan, S.C. Peter, Thermochemical CO_2 Hydrogenation to Single Carbon Products: Scientific and Technological Challenges. ACS Energy Lett., 3 (2018) 1938-1966.

[3] G.A. Olah, A. Goeppert, G.K.S. Prakash, Chemical recycling of carbon dioxide to methanol and dimethyl ether: From greenhouse gas to renewable, environmentally carbon neutral fuels and synthetic hydrocarbons. J. Org. Chem., 74 (2009) 487-498.

[4] T.A. Semelsberger, R. L. Borup, H. L. Greene, Dimethyl ether (DME) as an alternative fuel. J. Power Sour., 156 (2006) 497-511.

[5] C. Arcoumanis, C. Bae, R. Crookes, E. Kinoshita, The potential of di-methyl ether (DME) as an alternative fuel for compression-ignition engines: A review. Fuel, 87 (2008) 1014-1030.

[6] M.Y. Kim, S.H. Yoon, B.W. Ryu, C.S. Lee, Combustion and emission characteristics of DME as an alternative fuel for compression ignition engines with a high pressure injection system. Fuel, 87 (2008) 2779-2786.

[7] R. Song, K. Li, Y. Feng, S. Liu, Performance and emission characteristics of DME engine with high ratio of EGR. Energy and Fuels, 23 (2009) 5460-5466.

[8] A. Lerner, M. J. Brear, J. S. Lacey, R. L. Gordon, P. A. Webley, Life cycle analysis (LCA) of low emission methanol and di-methyl ether (DME) derived from natural gas. Fuel, 220 (2018) 871-878.

[9] A.S. Al-Dughaither, H. de Lasa, Neat dimethyl ether conversion to olefins (DTO) over HZSM-5: Effect of SiO_2/Al_2O_3 on porosity, surface chemistry, and reactivity. Fuel, 138 (2014) 52-64.

[10] P. Pérez-Uriarte, A. Ateka, A.T. Aguayo, J. Bilbao, Comparison of HZSM-5 Zeolite and SAPO (-18 and -34) Based Catalysts for the Production of Light Olefins from DME. Catal. Lett., 146 (2016) 1892-1902.

[11] P. Pérez-Uriarte, A. Ateka, M. Gamero, A.T. Aguayo, J. Bilbao, Effect of the Operating Conditions in the Transformation of DME to olefins over a HZSM-5 Zeolite Catalyst. Ind. Eng. Chem. Res., 55 (2016) 6569-6578.

[12] P. Pérez-Uriarte, M. Gamero, A. Ateka, M. Díaz, A.T. Aguayo, J. Bilbao, Effect of the Acidity of HZSM-5 Zeolite and the Binder in the DME Transformation to Olefins. Ind. Eng. Chem. Res., 55 (2016) 1513-1521.

[13] P. Pérez-Uriarte, A. Ateka, A.T. Aguayo, A. G. Gayubo, J. Bilbao, Kinetic model for the reaction of DME to olefins over a HZSM-5 zeolite catalyst. Chem. Eng. J., 302 (2016) 801-810.

[14] Z. Wen, Z. Li, Q. Ge, Y. Zhou, J. Sun, H: Abroshan, G. Li, Robust nickel cluster@Mes-HZSM-5 composite nanostructure with enhanced catalytic activity in the DTG reaction. J. Catal., 363 (2018) 26-33.

[15] K. Faungnawakij, N. Shimoda, T. Fukunaga, R. Kikuchi, K. Eguchi, Cu-based spinel catalysts CuB_2O_4 (B = Fe, Mn, Cr, Ga, Al, Fe0.75Mn0.25) for steam reforming of dimethyl ether. Appl. Catal. A Gen., 341 (2008) 139-145.

[16] K. Faungnawakij, N. Shimoda, N. Viriya-empikul, R. Kikuchi, K. Eguchi, Limiting mechanisms in catalytic steam reforming of dimethyl ether. Appl. Catal. B Environ., 97 (2010) 21-27.

[17] N. Shimoda, H. Muroyama, T. Matsui, K. Faungnawakij, R. Kikuchi, K. Eguchi, Dimethyl ether steam reforming under daily start-up and shut-down (DSS)-like operation over $CuFe_2O_4$ spinel and alumina composite catalysts. Appl. Catal. A Gen., 409-410 (2011) 91-98.

[18] L. Oar-Arteta, A. Remiro, A.T. Aguayo, J. Bilbao, A.G. Gayubo, Effect of Operating Conditions on Dimethyl Ether Steam Reforming over a $CuFe_2O_4$/γ-Al_2O_3 Bifunctional Catalyst. Ind. Eng. Chem. Res., 54 (2015) 9722-9732.

[19] L. Oar-Arteta, A.T. Aguayo, A: Remiro, A. Arandia, J. Bilbao, A.G. Gayubo, Kinetics of the steam reforming of dimethyl ether over $CuFe_2O_4$/γ-Al_2O_3. Chem. Eng. J., 306 (2016) 401-412.

[20] L. Oar-Arteta, A: Remiro, F. Epron, N. Bion, A.T. Aguayo, J. Biolbao, A.G. Gayubo, Comparison of Noble Metal- and Copper-Based Catalysts for the Step of Methanol Steam Reforming in the Dimethyl Ether Steam Reforming Process. Ind. Eng. Chem. Res., 55 (2016) 3546-3555.

[21] F. Trippe, M. Fröhling, F. Schultmann, R. Stahl, E. Henrich, A. Dalai, Comprehensive techno-economic assessment of dimethyl ether (DME) synthesis and Fischer–Tropsch synthesis as alternative process steps within biomass-to-liquid production. Fuel Process. Technol., 106 (2013) 577-586.

[22] S. Bhattacharya, K. B. Kabir, K. Hein, Dimethyl ether synthesis from Victorian brown coal through gasification – Current status, and research and development needs. Prog. Energy Comb. Sci., 39 (2013) 577-605.

[23] Z. Azizi, M. Rezaeimanesh, T. Tohidian, M.R. Rahimpour, Dimethyl ether: A review of technologies and production challenges. Chem. Eng. Process. Process Intensif., 82 (2014) 150-172.

[24] A. Molino, V. Larocca, S. Chianese, D. Musmarra, Biofuels production by biomass gasification: A review. Energies 11 (2018).

[25] G. R. Moradi, S. Nosrati, F. Yaripor, Effect of the hybrid catalysts preparation method upon direct synthesis of dimethyl ether from synthesis gas. Catal. Commun., 8 (2007) 598-606.

[26] A. Ateka, I. Sierra, J. Ereña, J. Bilbao, A.T. Aguayo, Performance of CuO–ZnO–ZrO_2 and CuO–ZnO–MnO as metallic functions and SAPO-18 as acid function of the catalyst for the synthesis of DME co-feeding CO_2. Fuel Process. Technol., 152 (2016) 34-45.

[27] Z. Li, J. Li, M. Dai, Y. Liu, D. Han, J. Wu, The effect of preparation method of the Cu–La_2O_3–ZrO_2/γ-Al_2O_3 hybrid catalysts on one-step synthesis of dimethyl ether from syngas. Fuel, 121 (2014) 173-177.

[28] J. Sun, G. Yang, Y. Yoneyama, N. Tsubaki, Catalysis chemistry of dimethyl ether synthesis. ACS Catal., 4 (2014) 3346-3356.

[29] J. Ereña, I. Sierra, M. Olazar, A.G. Gayubo, A.T. Aguayo, Deactivation of a CuO - ZnO - Al_2O_3/γ-Al_2O_3 catalyst in the synthesis of dimethyl ether. Ind. Eng. Chem. Res., 47 (2008) 2238-2247.

[30] A. García-Trenco, A. Vidal-Moya, A. Martínez, Study of the interaction between components in hybrid CuZnAl/HZSM-5 catalysts and its impact in the syngas-to-DME reaction. Catal. Today, 179 (2012) 43-51.

[31] I. Sierra, J. Ereña, A.T. Aguayo, J.M. Arandes, M. Olazar, J. Bilbao, Co-feeding water to attenuate deactivation of the catalyst metallic function (CuO–ZnO–Al_2O_3) by coke in the direct synthesis of dimethyl ether. Appl. Catal. B Environ., 106 (2011) 167-173.

[32] I. Sierra, J. Ereña, A.T. Aguayo, J.M. Arandes, J. Bilbao, Regeneration of $CuO\text{-}ZnO\text{-}Al_2O_3/\gamma\text{-}Al_2O_3$ catalyst in the direct synthesis of dimethyl ether. Appl. Catal. B Environ., 94 (2010) 108-116.

[33] G. Jia, Y. Tan, Y. Han, A comparative study on the thermodynamics of dimethyl ether synthesis from CO hydrogenation and CO_2 hydrogenation. Ind. Eng. Chem. Res., 45 (2006) 1152-1159.

[34] A.T. AguayoJ. Ereña, M. Mier, J.M. Arandes M. Olazar, J. Bilbao, Kinetic modeling of dimethyl ether synthesis in a single step on a $CuO\text{-}ZnO\text{-}Al_2O_3/\gamma\text{-}Al_2O_3$ catalyst. Ind. Eng. Chem. Res., 46 (2007) 5522-5530.

[35] A. Ateka, P. Pérez-Uriarte, M. Gamero, J. Ereña, A.T: Aguayo, J. Bilbao, A comparative thermodynamic study on the CO_2 conversion in the synthesis of methanol and of DME. Energy, 120 (2017) 796-804.

[36] Z.-z. Qin, X.-h. Zhou, T.-m. Su, Y.-x. Jiang, H.-b. Ji, Hydrogenation of CO_2 to dimethyl ether on La-, Ce-modified Cu-Fe/HZSM-5 catalysts. Catal. Commun., 75 (2016) 78-82.

[37] X. Zhou, T. Su, Y. Jiang, Z. Qin, H. Ji, Z. Guo, $CuO\text{-}Fe_2O_3\text{-}CeO_2$/HZSM-5 bifunctional catalyst hydrogenated CO_2 for enhanced dimethyl ether synthesis. Chem. Eng. Sci., 153 (2016) 10-20.

[38] F. Arena, G. Italiano, K. Barbera, G. Bonura, L. Spadaro, F. Frusteri, Basic evidences for methanol-synthesis catalyst design. Catal. Today, 143 (2009) 80-85.

[39] Y.J. Zhang, D.B Li, D. Jiang, Y. Zhu, Y. Wu, S.J. Zhang, K.J. Wang, J. Wu, Effect of Mn promoter on structure and properties of Mn modified $CuO\text{-}ZnO\text{-}ZrO_2$ /HZSM-5 catalysts for synthesis of dimethyl ether from CO_2 hydrogenation. J. Molec. Catal., 28 (2014) 344-350.

[40] X. D. Peng, A.W. Wang, B.A. Toseland, P.J.A. Tijm, Single-step syngas-to-dimethyl ether processes for optimal productivity, minimal emissions, and natural gas-derived syngas. Ind. Eng. Chem. Res., 38 (1999) 4381-4388.

[41] K. Sun, W. Lu, M. Wang, X. Xu, Low-temperature synthesis of DME from CO_2/H_2 over Pd-modified $CuO\text{-}ZnO\text{-}Al_2O_3\text{-}ZrO_2$/HZSM-5 catalysts. Catal. Commun., 5 (2004) 367-370.

[42] X. An, Y. Z. Zuo, Q. Zhang, D. Z. Wang, J. F. Wang, Dimethyl ether synthesis from CO_2 hydrogenation on a $CuO\text{-}ZnO\text{-}Al_2O_3\text{-}ZrO_2$/HZSM-5 bifunctional catalyst. Ind. Eng. Chem. Res., 47 (2008) 6547-6554.

[43] F. Frusteri, G.Bonura, C. Cannilla, G. Drago Ferrante, A. Aloise, E. Catizzone, M. Migliori, G. Giordano, Stepwise tuning of metal-oxide and acid sites of CuZnZr-MFI hybrid catalysts for the direct DME synthesis by CO_2 hydrogenation. Appl. Catal. B Environ., 176–177 (2015) 522-531.

[44] F. Frusteri, M. Migliori, C. Cannilla, L. Frusteri, E. Catizzone, A. Aloise, G. Giordano, G. Bonura, Direct CO_2-to-DME hydrogenation reaction: New evidences of a superior behaviour of FER-based hybrid systems to obtain high DME yield. J. CO2 Utilization, 18 (2017) 353-361.

[45] Y. Suwannapichat, T. Numpilai, N. Chanlek, K. Faungnawakij, M. Chareonpanich, J. Limtrakul, T. Witoon, Direct synthesis of dimethyl ether from CO_2 hydrogenation over novel hybrid catalysts containing a $Cu–ZnO–ZrO_2$ catalyst admixed with WO_x/Al_2O_3 catalysts: Effects of pore size of Al_2O_3 support and W loading content. Energy Convers. Manage., 159 (2018) 20-29.

[46] M.-H. Zhang, Z.-M. Liu, G.-D. Lin, H.-B. Zhang, Pd/CNT-promoted CuZrO2/HZSM-5 hybrid catalysts for direct synthesis of DME from CO_2/H_2. Appl. Catal. A Gen., 451 (2013) 28-35.

[47] M. Cai, A. Palcic, V. Subramanian, S. Moldovan, O. Ersen, V. Valtchev, V.V. Ordomsky, A.Y. Khodakov, Direct dimethyl ether synthesis from syngas on copper–zeolite hybrid catalysts with a wide range of zeolite particle sizes. J. Catal., 338 (2016) 227-238.

[48] R. Phienluphon, K. Pinkaew, G. Yang, J. Li, Q. Wei, Y. Yoneyama, T. Vitidsant, N. Tsubaki, Designing core ($Cu/ZnO/Al_2O_3$)–shell (SAPO-11) zeolite capsule catalyst with a facile physical way for dimethyl ether direct synthesis from syngas. Chem. Eng. J., 270 (2015) 605-611.

[49] A. Ateka, P. Pérez-Uriarte, I. Sierra, J. Ereña, J. Bilbao, A.T. Aguayo, Regenerability of the CuO–ZnO–MnO/SAPO-18 catalyst used in the synthesis of dimethyl ether in a single step. React. Kinet. Mech. Catal., 119 (2016) 655-670.

[50] A. Ateka, P. Pérez-Uriarte, M. Sánchez-Contador, J.Ereña, A.T. Aguayo, J. Bilbao, Direct synthesis of dimethyl ether from syngas on CuO-ZnO-MnO/SAPO-18 bifunctional catalyst. Int. J. Hydrogen Energy, 41 (2016) 18015-18026.

[51] M. Sánchez-Contador, A. Ateka, A.T. Aguayo, J. Bilbao, Behavior of SAPO-11 as acid function in the direct synthesis of dimethyl ether from syngas and CO_2. J. Ind. Eng. Chem., 63 (2018) 245-254.

[52] T. Witoon, P. Kidkhunthod, M. Chareonpanich, J. Limtrakul, Direct synthesis of dimethyl ether from CO_2 and H_2 over novel bifunctional catalysts containing $CuO-ZnO-ZrO_2$ catalyst admixed with WO_x/ZrO_2 catalysts. Chem. Eng. J., 348 (2018) 713-722.

[53] A. Ateka, J. Ereña, M. Sánchez-Contador, P. Pérez-Uriarte, J. Bilbao, A.T. Aguayo, Capability of the direct dimethyl ether synthesis process for the conversion of carbon dioxide. Appl. Sci., 8 (2018) 677.

[54] J. Ereña, I. Sierra, A.T. Aguayo, A. Ateka, M. Olaza, J. Bilbao, Kinetic modelling of dimethyl ether synthesis from (H_2+CO_2) by considering catalyst deactivation. Chem. Eng. J., 174 (2011) 660-667.

[55] R. Peláez, P. Marín, F.V. Díez, S. Ordóñez, Direct synthesis of dimethyl ether in multi-tubular fixed-bed reactors: 2D multi-scale modelling and optimum design. Fuel Process. Technol., 174 (2018) 149-157.

[56] M. De Falco, M. Capocelli, G. Centi, Dimethyl ether production from CO_2 rich feedstocks in a one-step process: Thermodynamic evaluation and reactor simulation. Chem. Eng. J., 294 (2016) 400-409.

[57] M. De Falco, M. Capocelli, Direct Synthesis of MEthanol and Dimethyl Ether From CO_2-rich Feedstocks: Thermodynamic Analysis and Selective Membrane Application.in Methanol: Science and Engineering. (2017), pp. 113-128.

[58] K.L. Ng, D. Chadwick, B.A. Toseland, Kinetics and modelling of dimethyl ether synthesis from synthesis gas. Chem. Eng. Sci. 54 (1999) 3587-3592.

[59] G.R. Moradi, J. Ahmadpour, F. Yaripour, Intrinsic kinetics study of LPDME process from syngas over bi-functional catalyst. Chem. Eng. J., 144 (2008) 88-95.

[60] G.H. Graaf, E.J. Stamhuis, A.A.C.M. Beenackers, Kinetics of low-pressure methanol synthesis. Chem. Eng. Sci., 43 (1988) 3185-3195.

[61] K.M.V. Bussche, G.F. Froment, A Steady-State Kinetic Model for Methanol Synthesis and the Water Gas Shift Reaction on a Commercial $Cu/ZnO/Al_2O$ Catalyst. J. Catal., 161 (1996) 1-10.

[62] G. Bercic, J. Levec, Intrinsic and global reaction rate of methanol dehydration over .gamma.-alumina pellets. Ind. Eng. Chem. Res., 31 (1992) 1035-1040.
[63] G. Bercic, J. Levec, Catalytic Dehydration of Methanol to Dimethyl Ether. Kinetic Investigation and Reactor Simulation. Ind. Eng. Chem. Res., 32 (1993) 2478-2484.
[64] G. Natta, Catalysis. P. H. Emmett, Ed., Reinhold, New York, 1955, vol. 3.
[65] P. Villa, P. Forzatti, G. Buzzi-Ferraris, G. Garone, I. Pasquon, Synthesis of alcohols from carbon oxides and hydrogen. 1. Kinetics of the low-pressure methanol synthesis. Ind. Eng. Chem. Process Design Develop., 24 (1985) 12-19.
[66] T. Shido, Y. Iwasawa, The Effect of Coadsorbates in Reverse Water-Gas Shift Reaction on ZnO, in Relation to Reactant-Promoted Reaction Mechanism. J. Catal. 140, 575-584 (1993).
[67] D.B. Clarke, A.T. Bell, An Infrared Study of Methanol Synthesis from CO_2 on Clean and Potassium-Promoted Cu/SiO_2. J. Catal., 154 (1995) 314-328.
[68] C. Rhodes, G.J. Hutchings, A. M. Ward, Water-gas shift reaction: finding the mechanistic boundary. Catal. Today, 23 (1995) 43-58.
[69] H.W. Lim, M.J. Park, S.H. Kang, H.J. Chae, J.W. Bae, K.W. Jun, Modeling of the kinetics for methanol synthesis using $Cu/ZnO/Al_2O_3/ZrO_2$ catalyst: Influence of carbon dioxide during hydrogenation. Ind. Eng. Chem. Res., 48 (2009) 10448-10455.
[70] R. Burch, A. Goguet, F.C. Meunier, A critical analysis of the experimental evidence for and against a formate mechanism for high activity water-gas shift catalysts. Appl. Catal. A Gen., 409-410 (2011) 3-12.
[71] A.R. De La Osa, A. De Lucas, A. Romero, J.L. Valverde, P. Sánchez, Kinetic models discrimination for the high pressure WGS reaction over a commercial CoMo catalyst. Int. J. Hydrogen Energy, 36 (2011) 9673-9684.
[72] Y.-F. Zhao, Y. Yang, C. Mims, C.H.F. Peden, J. Li, D. Mei, Insight into methanol synthesis from CO_2 hydrogenation on Cu(1 1 1): Complex reaction network and the effects of H_2O. J. Catal., 281 (2011) 199-211.
[73] L.C. Grabow, M. Mavrikakis, Mechanism of methanol synthesis on cu through CO_2 and CO hydrogenation. ACS Catal., 1 (2011) 365-384.
[74] Y. Yang, C.A. Mims, D.H. Mei, C.H.F. Peden, C.T. Campbell, Mechanistic studies of methanol synthesis over Cu from $CO/CO_2/H_2/H_2O$ mixtures: The source of C in methanol and the role of water. J. Catal., 298 (2013) 10-17.
[75] I. Sierra, J. Ereña, A.T. Aguayo, M. Olazar, J. Bilbao, Deactivation kinetics for direct dimethyl ether synthesis on a $CuO-ZnO-Al_2O_3/\gamma-Al_2O_3$ Catalyst. Ind. Eng. Chem. Res., 49 (2010) 481-489.
[76] J. Ereña, J.M. Arandes, J. Bilbao, A.T. Aguayo, H.I. De Lasa, Study of Physical Mixtures of Cr_2O_3-ZnO and ZSM-5 Catalysts for the Transformation of Syngas into Liquid Hydrocarbons. Ind. Eng. Chem. Res., 37 (1998) 1211-1219.
[77] J. Pérez-Ramírez, R.J. Berger, G. Mul, F. Kapteijn, J.A. Moulijn, The six-flow reactor technology: A review on fast catalyst screning and kinetic studies. Catal. Today, 60 (2000) 90-109.
[78] D. Mier, A.T. Aguayo, M. Gamero, A.G. Gayubo, J. Bilbao, Kinetic modeling of n-butane cracking on HZSM-5 zeolite catalyst. Ind. Eng. Chem. Res., 49 (2010) 8415-8423.

[79] A.G. Gayubo, A. Alonso, B. Valle, A.T. Aguayo, J. Bilbao, Kinetic model for the transformation of bioethanol into olefins over a HZSM-5 zeolite treated with alkali. Ind. Eng. Chem. Res., 49 (2010) 10836-10844.

[80] E. Epelde, A.T. Aguayo, M. Olazar, J. Bilbao, A.G. Gayubo, Kinetic model for the transformation of 1-butene on a K-modified HZSM-5 catalyst. Ind. Eng. Chem. Res., 53 (2014) 10599-10607.

[81] K. Toch, J.W. Thybaut, G.B. Marin, A systematic methodology for kinetic modeling of chemical reactions applied to n-hexane hydroisomerization. AIChE J., 61 (2015) 880-892.

[82] T. Cordero-Lanzac, A.T. Aguayo, A.G. Gayubo, P. Castaño, J. Bilbao, Simultaneous modeling of the kinetics for n-pentane cracking and the deactivation of a HZSM-5 based catalyst. Chem. Eng. J., 331 (2018) 818-830.

[83] A.K. Agarwal, M.L. Brisk, Sequential Experimental Design for Precise Parameter Estimation. 1. Use of Reparameterization. Ind. Eng. Chem. Process Design Develop., 24 (1985) 203-207.

[84] A.G. Gayubo, A.T. Aguayo, A.E. Sánchez Del Campo, A. M. Tarrío, J. Bilbao, Kinetic modeling of methanol transformation into olefins on a SAPO-34 catalyst. Ind. Eng. Chem. Res., 39 (2000) 292-300.

[85] A.G. Gayubo, A.T. Aguayo, A. Alonso, J. Bilbao, Kinetic modeling of the methanol-to-olefins process on a silicoaluminophosphate (SAPO-18) catalyst by considering deactivation and the formation of individual olefins. Ind. Eng. Chem. Res., 46 (2007) 1981-1989.

[86] A.G. Gayubo, A. Alonso, B. Valle, A.T. Aguayo, M. olazar, J. Bilbao, Kinetic modelling for the transformation of bioethanol into olefins on a hydrothermally stable Ni–HZSM-5 catalyst considering the deactivation by coke. Chem. Eng. J., 167 (2011) 262-277.

[87] D.A. Coley, An Introduction to Genetic Algorithms for Scientists and Engineers. World Scientific Publishing Company, Singapore, 2003.

[88] A. Ateka, J. Ereña, P. Pérez-Uriarte, A.T. Aguayo, J. Bilbao, Effect of the content of CO_2 and H_2 in the feed on the conversion of CO_2 in the direct synthesis of dimethyl ether over a CuO-ZnO-Al_2O_3/SAPO-18 catalyst. Int. J. Hydrogen Energy, 42 (2017) 27130-27138.

[89] I. Banu, R. Ganea, G. Vasilievici, A. Anghel, V. Gogulancea, G. Isopencu, G. Bozga, An evaluation of published kinetic models for vapor phase methanol conversion to dimethyl ether over the H-ZSM-5 catalyst. Energy Fuel., 347 (2018) 741-753.

[90] C. Ortega, M. Rezaei, V. Hessel, G. Kolb, Methanol to dimethyl ether conversion over a ZSM-5 catalyst: Intrinsic kinetic study on an external recycle reactor. Chem. Eng. J., 347 (2018) 741-753.

[91] A. Hadipour, M. Sohrabi, Synthesis of some bifunctional catalysts and determination of kinetic parameters for direct conversion of syngas to dimethyl ether. Chem. Eng. J. 137 (2008) 294-301.

[92] K. Stangeland, H. Li, Z. Yu, Thermodynamic Analysis of Chemical and Phase Equilibria in CO_2 Hydrogenation to Methanol, Dimethyl Ether, and Higher Alcohols. Ind. Eng. Chem. Res., 57 (2018) 4081-4094.

WEB REFERENCES

Climate change: http://www.epa.gov/climatechange/ghgemissions/gases(co2.html) (2018, 5th January).